ACS NANO

www.acsnano.org

Article

NaF@MnO-Based Sacrificial Cathode/Separator Composite for Boosting the Energy Density of Sodium-Ion Batteries

Sang Jae Park,[#] Sang-Yeop Lee,[#] Yong Min Kim,[#] Jungmin Kang, Jae Kwon Seo, Young-Jun Kim,* Jongsoon Kim,* and Ki Jae Kim*

Cite This: *ACS Nano* 2026, 20, 4799–4807

Read Online

ACCESS | Metrics & More | Article Recommendations | Supporting Information

ABSTRACT: Growing concerns over lithium cost and supply limitations have led to increasing interest in sodium-ion batteries (SIBs). However, hard carbon (HC) anodes suffer from low initial Coulombic efficiency due to irreversible sodium loss during the formation of the solid electrolyte interphase and ion trapping, which reduces the useable capacity in full-cell systems. Various sacrificial sodium sources have been investigated, but many generate gas, react with moisture, or degrade the cathode when they are mixed directly with it. In this study, we present a presodiation strategy based on a MnO@NaF composite (MNC) coated onto the cathode-facing side of the separator (MNCS). They are inexpensive, stable in air, and compatible with standard electrode fabrication processes. The MNC releases additional sodium through NaF decomposition catalyzed by MnO with negligible gaseous byproducts. By placing the MNC on the separator rather than on the cathode, the design avoids unwanted reactions while improving sodium availability and ion transport. When applied to a full cell with an O3-type $Na[Li_{0.05}(Ni_{0.25}Fe_{0.25}Mn_{0.5})_{0.95}]O_2$ cathode and HC anode, the MNCS increased the initial discharge capacity to 169.5 mAh g^{-1} and maintained 69.5% of its capacity after 200 cycles. These results demonstrate the effectiveness of this approach in improving the available energy density and long-term stability in SIBs.

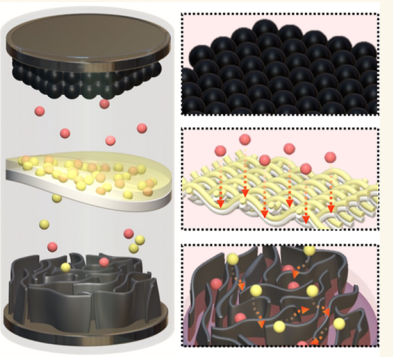

KEYWORDS: *Na-ion batteries, MnO@NaF composite, functional separator, presodiation, high-energy density*

INTRODUCTION

The growing demand for large-scale energy storage has intensified the development of cost-effective and sustainable battery technologies. Sodium-ion batteries (SIBs) have emerged as a promising alternative to lithium-ion batteries (LIBs), benefiting from the abundance and low cost of sodium resources, along with similar alkali-ion-based reaction mechanisms.[1] Owing to these advantages, a wide range of studies has focused on developing suitable cathode and anode materials for SIBs.[2]

On the anode side, hard carbon (HC) is widely studied due to its low cost and ability to store a large amount of Na^+ ions.[3] In terms of graphite, although it is widely used in LIBs, it cannot accommodate Na ions effectively in carbonate-based electrolytes, primarily due to their larger ionic radius and poor intercalation into graphitic layers.[4]

While HC is considered the most practical anode for SIBs, it suffers from a critical drawback, low initial Coulombic efficiency (ICE). This limitation originates from the irreversible consumption of Na ions during the first cycle, primarily due to the formation of a solid electrolyte interphase (SEI) and Na trapping in closed micropores.[5] The resulting initial capacity loss (ICL) reduces the number of active Na^+ ions available for subsequent cycles and causes a noticeable decline in the energy density of full-cells.[6] This remains a key challenge to be addressed in the practical implementation of HC-based SIBs.

To mitigate this issue, various presodiation strategies using sacrificial sodium sources have been proposed.[7] While Na-metal precycling or chemical sodiation can restore the Na balance at the anode, their implementation is limited by air sensitivity and added processing complexity. Alternatively, cathode-side sacrificial additives such as Na_2CO_3,[8] $Na_2C_4O_4$,[9] $NaNO_2$,[10] Na_3PS_3O,[11] and Na_3P[12] have been introduced to supply excess Na during initial charging. However, many of these compounds suffer from critical drawbacks: they produce gaseous byproducts such as CO_2, NO_x, etc., which raise internal cell pressure; they leave behind electrochemically inactive residues; and they often react strongly with moisture, making them difficult to handle under dry-room conditions.[13]

In this study, we report a gas-free and separator-applied sacrificial sodium source based on a MnO@NaF composite (MNC), designed to overcome both electrochemical and

Received: September 23, 2025
Revised: January 27, 2026
Accepted: January 28, 2026
Published: February 5, 2026

https://doi.org/10.1021/acsnano.5c16400
ACS Nano 2026, 20, 4799–4807

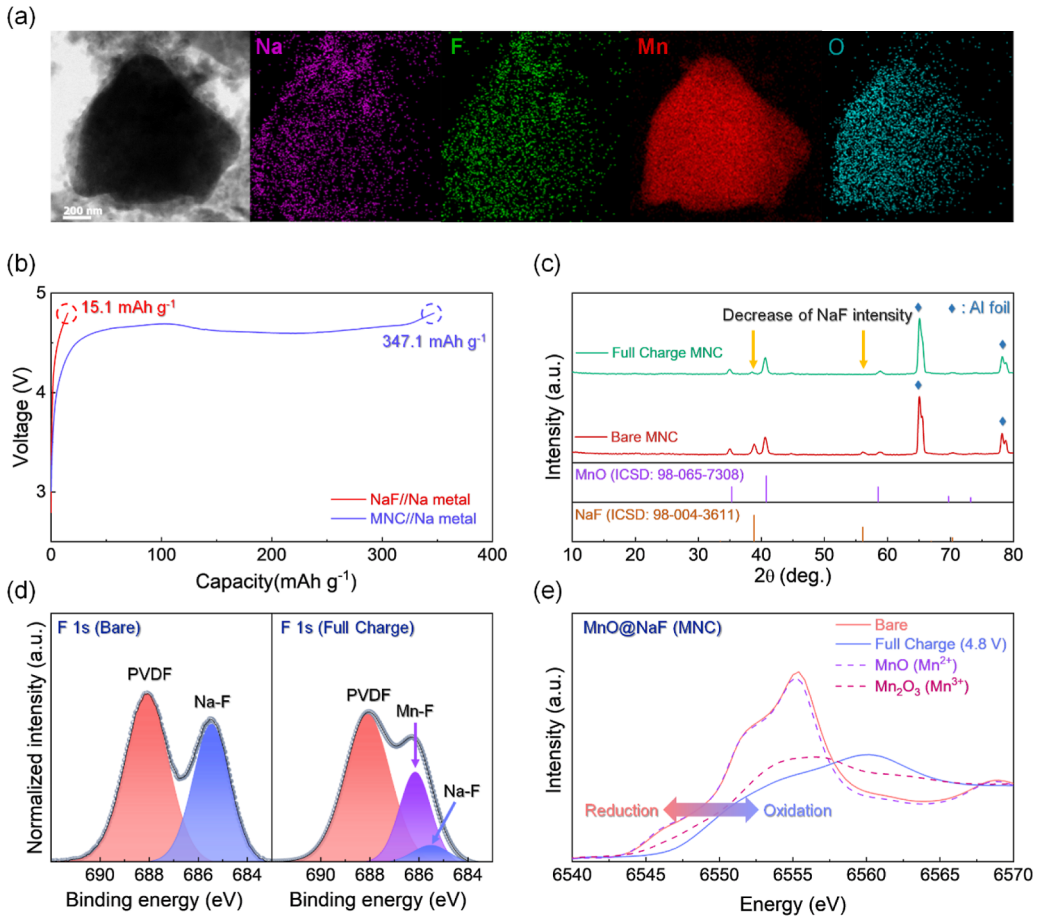

Figure 1. (a) TEM image and EDS mapping results of the MNC with Na, F, Mn, and O elements. (b) Galvanostatic charge profiles of the NaF and MNC at 20 mA g^{-1}. (c) XRD patterns of the MNC and charge MNC in the range of 10°−80°. (d) The F 1s XPS spectra of MNC and charge MNC. (e) Mn K-edge XANES analyses of the MNC and Full charge MNC.

practical limitations associated with conventional presodiation materials. NaF provides additional Na through electrochemical decomposition, while MnO plays a dual role by promoting NaF activation and scavenging the resulting fluoride ions to suppress unwanted side reactions at the cathode−electrolyte interface.

Unlike previous methods that involve mixing sacrificial materials directly into the cathode, which can degrade conductivity and electrochemical activity, our approach coats the MNC onto the cathode-facing side of the separator. This configuration physically separates the sacrificial reaction from the active cathode, allowing localized Na release without interfering with the cathode performance. The MNC layer can be applied using conventional slurry processes and is stable under dry-room conditions, making it suitable for practical cell manufacturing.

When applied in a full-cell consisting of an O3-type $Na[Li_{0.05}(Ni_{0.25}Fe_{0.25}Mn_{0.5})_{0.95}]O_2$ (O3-NLNFM) cathode, MNC-coated separator (MNCS), and HC anode, the system delivered an initial discharge capacity of approximately 169.5 mAh g^{-1}. This value is more than double that of the control cell with a pristine separator, which showed only about 104.0 mAh g^{-1}, clearly demonstrating the effectiveness of the MNCS in compensating for initial sodium loss and enhancing energy output. In addition to the increased available capacity under the full-cell system, the O3-NLNFM//MNCS//HC full-cell exhibited significantly improved rate capability and cycling stability. In the case of high-rate operation at 8C, the O3-NLNFM//MNCS//HC full cell retained 52.6% of its initial capacity, whereas the control cell (O3-NLNFM//HC) retained only 44.5%. After 200 cycles at 0.5C, the O3-NLNFM//MNCS//HC full cell maintained a capacity retention of 69.5%, clearly outperforming the control cell.

Overall, this work presents a practical presodiation strategy that addresses both the electrochemical and processing limitations of current SIB systems. By effectively compensating for the initial sodium loss in hard carbon anodes, the separator-integrated MnO@NaF approach offers a promising route toward improving the energy density of sodium-ion batteries.

RESULTS AND DISCUSSION

Properties of the MnO@NaF Composite (NMC) as Presodiation Materials

The NaF has a high theoretical capacity of 638 mAh g^{-1}, making it a promising candidate for use as a sacrificial sodium source in presodiation strategies. In addition to its high capacity, NaF is chemically stable in air and commercially available at a low cost. However, its practical use is limited by its high decomposition potential (~5.9 V vs. Na^+/Na), which prevents effective activation under typical electrochemical conditions.[14] To overcome this issue, MnO, an inexpensive and air-stable metal oxide, was introduced to promote the electrochemical decomposition of NaF by catalytic activation.[15]

https://doi.org/10.1021/acsnano.5c16400
ACS Nano 2026, 20, 4799−4807

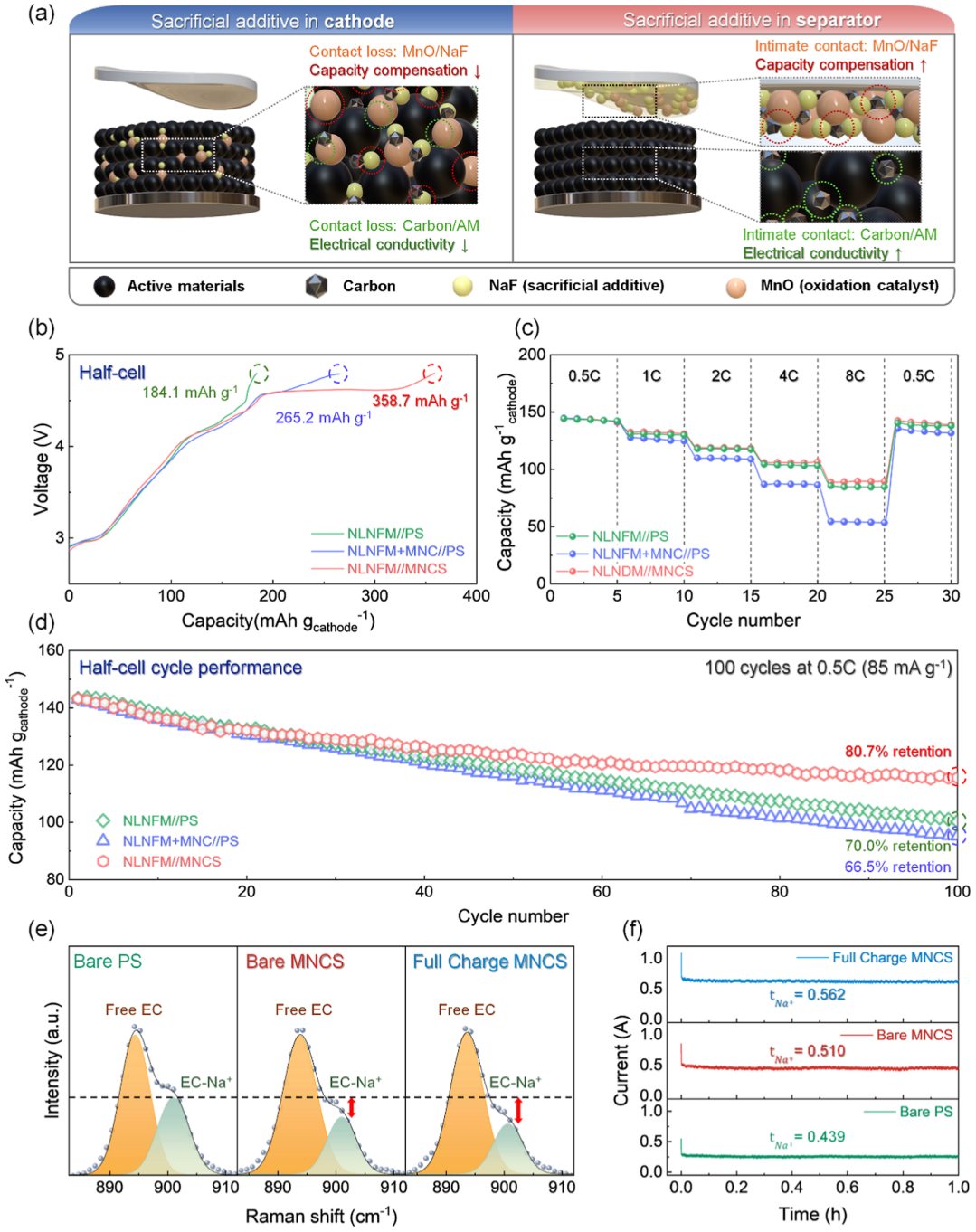

Figure 2. (a) Schematics comparing presodiation as a cathode additive and presodiation as a separator coating. (b) Galvanostatic charge profiles of the Na metal half-cell for the first cycle (c) rate performance of the Na metal half-cell with several cycles at various current densities. (d) Cycling performance of the half-cell at 0.5C. (e) Raman spectra of the electrolyte wetted bare PS, bare MNCS, and charge MNCS. (f) Measured Na^+ transference numbers for the bare PS, bare MNCS, and charge MNCS.

Since NaF has a low electronic conductivity, it is important to increase the contact area between NaF and MnO and improve the overall conductivity of the composite. A high-energy ball milling process was applied to reduce the particle sizes of MnO and NaF, enhance their interfacial contact, and mix them uniformly with Super P as a conductive additive. The resulting MnO@NaF composite (MNC) was prepared by ball milling at 500 rpm for 12 h and used as a presodiation material.

X-ray diffraction (XRD) analysis confirmed that the crystal structures of both NaF and MnO remained intact after ball milling (Figure S1), indicating that the mechanical process did not alter the phase of each component. Scanning transmission electron microscopy (STEM) and elemental mapping based on energy-dispersive X-ray spectroscopy (EDS) results showed that NaF particles were well distributed on the surface of MnO, with an overall composite particle size of around 1 μm (Figure 1a). The uniform interfacial contact between NaF and MnO formed by ball milling increases the reactive surface area, which is expected to promote the catalytic decomposition of NaF. Super P was also evenly dispersed throughout the composite, improving the electronic conductivity of the otherwise insulating components.

https://doi.org/10.1021/acsnano.5c16400
ACS Nano 2026, 20, 4799−4807

To compare the electrochemical performance of MNC with that of pristine NaF, galvanostatic charging tests were conducted in Na-metal half-cells using each material as the cathode. As shown in Figure 1b, the NaF electrode exhibited negligible charge capacity up to 4.8 V, consistent with its high decomposition potential and limited electrochemical activity. In contrast, the MNC delivered a charge capacity of 347.1 mAh g^{-1}, indicating that the incorporation of MnO enabled the facile decomposition of NaF and the release of active sodium during the charging process. Moreover, after the first charge, the MNCS-based cell retained less than 12.6% of the initial capacity, confirming that the sacrificial material had been largely consumed during the initial cycle (Figure S2). These results demonstrate that MNCS effectively supplies active sodium during formation and becomes electrochemically inactive in subsequent cycles.

To investigate the decomposition mechanism of NaF in the MNC during charge, we performed various ex situ analyses, including XRD, X-ray photoelectron spectroscopy (XPS), and X-ray absorption near edge structure (XANES). As shown in Figure 1c, the ex situ XRD results revealed that the characteristic diffraction peaks of NaF diminished significantly after charging at 4.8 V, indicating the decomposition of NaF after the charging process. This structural change corresponds to the observed charge capacity as the decomposition of NaF contributes to the release of additional active Na^+ ions. In contrast, the diffraction peaks of MnO remained well after the charging process, suggesting that MnO underwent negligible structural changes during the process, further supporting the role of its catalytic effect in facilitating the decomposition of NaF.

Further insights into the chemical changes were obtained from the F 1s XPS spectra (Figure 1d). Before charging, distinct peaks corresponding to Na−F[16] and PVDF[17] were observed. After charging, peaks decreased notably, accompanied by the emergence of a Mn−F peak,[18] confirming the formation of Mn−F bonds. This result indicates that MnO actively participated in the reaction, likely by accepting fluoride ions during NaF decomposition. Additionally, ex situ Mn K-edge XANES analyses revealed clear oxidation in Mn ions after charging, further supporting the redox involvement of Mn in the catalytic process of MnO (Figure 1e).

These results confirm that MnO actively promotes the decomposition of NaF, not only by providing catalytic surface contact but also by participating in charge transfer and stabilizing fluoride species through Mn−F bond formation. This catalytic effect reduces the decomposition voltage and enables the effective release of sodium during charging, as described by the following reaction:

$$\mathrm{MnO} + x\mathrm{NaF} \rightarrow \mathrm{MnOF}_x + x\mathrm{Na}^+ + x\mathrm{e}^- \quad (1)$$

Fabrication of MNC-Coated Separators (MNCSs) and Half-Cell Tests

To apply the MNC as a sacrificial sodium source in a practical cell design, we adopted a separator-coated configuration rather than the conventional cathode-additive approach. As schematically illustrated in Figure 2a, directly mixing presodiation materials such as NaF@MnO into the cathode can lead to electronic isolation of the sacrificial component due to its low intrinsic conductivity and limited contact with conductive pathways in the slurry-processed electrode. This can result in incomplete decomposition and an inefficient sodium release. In contrast, coating the MNC onto the separator provides a more continuous and conductive network within the sacrificial layer, ensuring uniform contact and efficient electrochemical activation while physically isolating it from the cathode. Based on this strategy, the MNC-coated separator (MNCS) was fabricated by blade-coating the MNC onto one side of a pristine separator (PS) using a slurry composed of poly(vinylidene fluoride) (PVDF) dissolved in *N*-methyl-2-pyrrolidone (NMP).

To evaluate the effectiveness of this approach, we conducted half-cell tests using an O3-type $Na[Li_{0.05}(Ni_{0.25}Fe_{0.25}Mn_{0.5})_{0.95}]O_2$ (O3-NLNFM) cathode as the working electrode and sodium metal as the counter/reference electrode. The half-cells were assembled with three different configurations: (i) a pristine separator (O3-NLNFM//PS), (ii) a pristine separator and a cathode incorporating MNC as an additive (O3-NLNFM + MNC//PS), and (iii) an MNC-coated separator (O3-NLNFM//MNCS). These comparisons were designed to isolate the effect of the MNC location within the cell configuration and validate the advantages of the separator-coated architecture.

Galvanostatic charge−discharge tests were performed at a current density of 20 mA g_{MNC}^{-1} with a voltage range of 1.95−4.8 V for the first cycle and 1.95−4.5 V for subsequent cycles. As shown in Figure 2b, the first charge profiles of the O3-NLNFM//PS, O3-NLNFM + MNC//PS, and the O3-NLNFM//MNCS half-cells showed nearly identical behavior up to 4.5 V, reflecting the intrinsic capacity contribution from the O3-NLNFM cathode. Above 4.5 V, however, additional capacity was observed only in the MNC-integrated cells, clearly indicating the contribution from the sacrificial cathode component. This difference demonstrates the activation of MNC and its contribution as an additional sodium source during the initial charging process.

Among the three configurations, the O3-NLNFM//MNCS cell exhibited the highest first charge capacity of 358.7 mAh g^{-1}, significantly surpassing the 265.2 mAh g^{-1} achieved by the O3-NLNFM + MNC//PS cell. This result indicates that applying the sacrificial cathode on the separator side is more effective for its electrochemical activation than direct mixing with the cathode, likely due to improved contact uniformity and minimized interference with the active cathode structure.

In addition to the initial charge performance, the MNCS-based cell also exhibited an outstanding rate capability and cycle performance. As shown in Figure 2c, under a high-rate condition of 8C (1C = 170 mA g^{-1}), the discharge capacities of O3-NLNFM//PS and O3-NLNFM + MNC//PS were 85.8 and 54.4 mAh g^{-1}, respectively, whereas O3-NLNFM//MNCS delivered 88.8 mAh g^{-1}. Moreover, after 100 cycles at 0.5C, the MNCS-based cell retained 80.7% of its capacity, outperforming both the capacity of the O3-NLNFM//PS and the capacity of the O3-NLNFM + MNC//PS cells (Figure 2d).

These results demonstrate that the MNCS strategy not only provides additional sodium during the initial charging process but also improves the rate capability and long-term cycling performance. Applying the sacrificial cathode onto the separator rather than blending it into the cathode offers a more efficient and scalable presodiation method for practical SIB systems.

The improved electrochemical performance can also be attributed to enhanced sodium ion transport within the cell, which is achieved through the introduction of the MNCS. Polar metal oxide coatings on separators are known to alter the

https://doi.org/10.1021/acsnano.5c16400
ACS Nano 2026, 20, 4799−4807

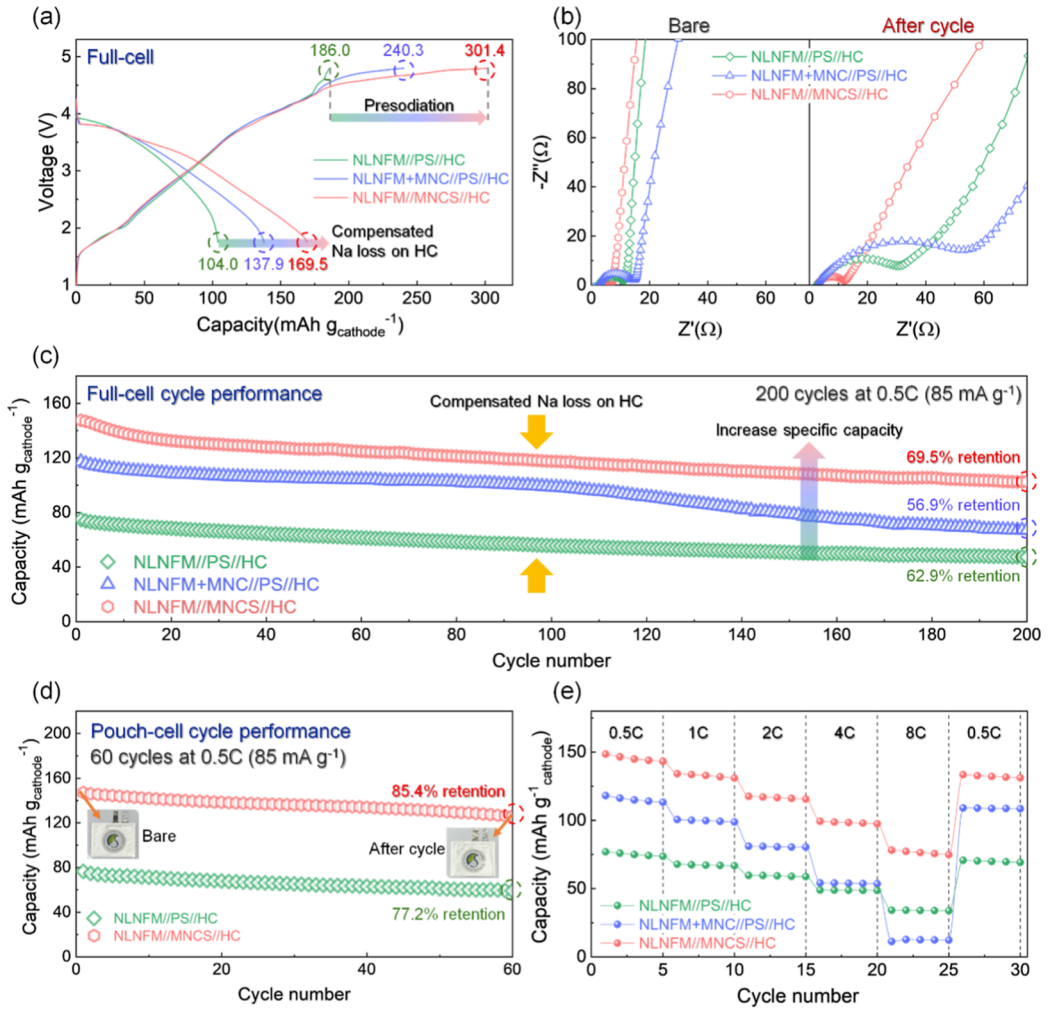

Figure 3. (a) Comparison of the charge/discharge voltage profiles of the full-cell during the first cycle. Nyquist plots of (b) bare full-cell and after the first cycle. (c) Cycling performance of the full-cell at 0.5C. (d) Cycling performance of the pouch cell at 0.5C, with an inset showing optical images of the pouch cell before and after cycling (the emblem shown in the pouch-cell photograph is the official logo of Sungkyunkwan university (SKKU) and is reproduced with permission). (e) Rate performance from 0.5 to 8C of the full-cell.

solvation structure of Na^+ ions in the electrolyte, which can enhance ion mobility.[19] To investigate this effect, we performed Raman spectroscopy on separators soaked in the electrolyte (Figure 2e). Both PS and MNCS exhibited two peaks at 893.8 cm^{-1} and 900.9 cm^{-1}, corresponding to free EC and EC-Na species, respectively. The EC-Na/EC intensity ratio decreased from 0.362 in PS to 0.300 in MNCS, indicating an increased fraction of free EC and thus enhanced Na^+ ion dissociation. After charging, the ratio further decreased to 0.274 due to the formation of polar $MnOF_x$ species. This trend suggests that MNCS promotes the availability of free Na^+ ions by modifying the local solvation environment.

To further evaluate the effect of MNC in a different configuration, we measured the electrode resistivity of the O3-NLNFM and the O3-NLNFM + MNC electrodes using an electrode measurement system (Figure S3). These results indicated that the O3-NLNFM + MNC electrode (2.25 and 0.36 Ω cm^2) exhibited significantly higher volume and surface resistance compared to the O3-NLNFM electrode (1.17 and 0.11 Ω cm^2). This increase in resistivity suggests that the inherently low electronic conductivity of MNC hinders electron transport when it is directly mixed into the cathode, which can negatively affect the overall electrochemical performance.

To quantify the effect on ion transport, the Na^+ ion transference number (t_{Na+}) was measured by using chronoamperometry (CA) and electrochemical impedance spectroscopy (EIS) in symmetric Na//Na cells. As shown in Figures 2f and S4, the t_{Na+} increased from 0.439 for the PS to 0.510 with the MNCS, indicating that the MNC coating facilitates greater dissociation of Na^+ ions by modifying the solvation environment at the separator interface. After charging, the t_{Na+} further increased to 0.562, which can be attributed to the formation of highly polar $MnOF_x$ species that enhance Na^+ ion mobility by further disrupting the ion−solvent coordination structure. These results confirm that the MNCS not only supplies active sodium during the initial cycle but also continuously improves ion transport through progressive solvation tuning.

In addition to functional advantages, the MNC was found to be compatible with conventional slurry processing. Unlike most presodiation additives, which raise the alkalinity of NMP-PVDF slurries and cause gelation, the MNC maintained a pH comparable to that of Super P (Figure S5). Visual and rheological evaluations confirmed that no gelation occurred

https://doi.org/10.1021/acsnano.5c16400
ACS Nano 2026, 20, 4799−4807

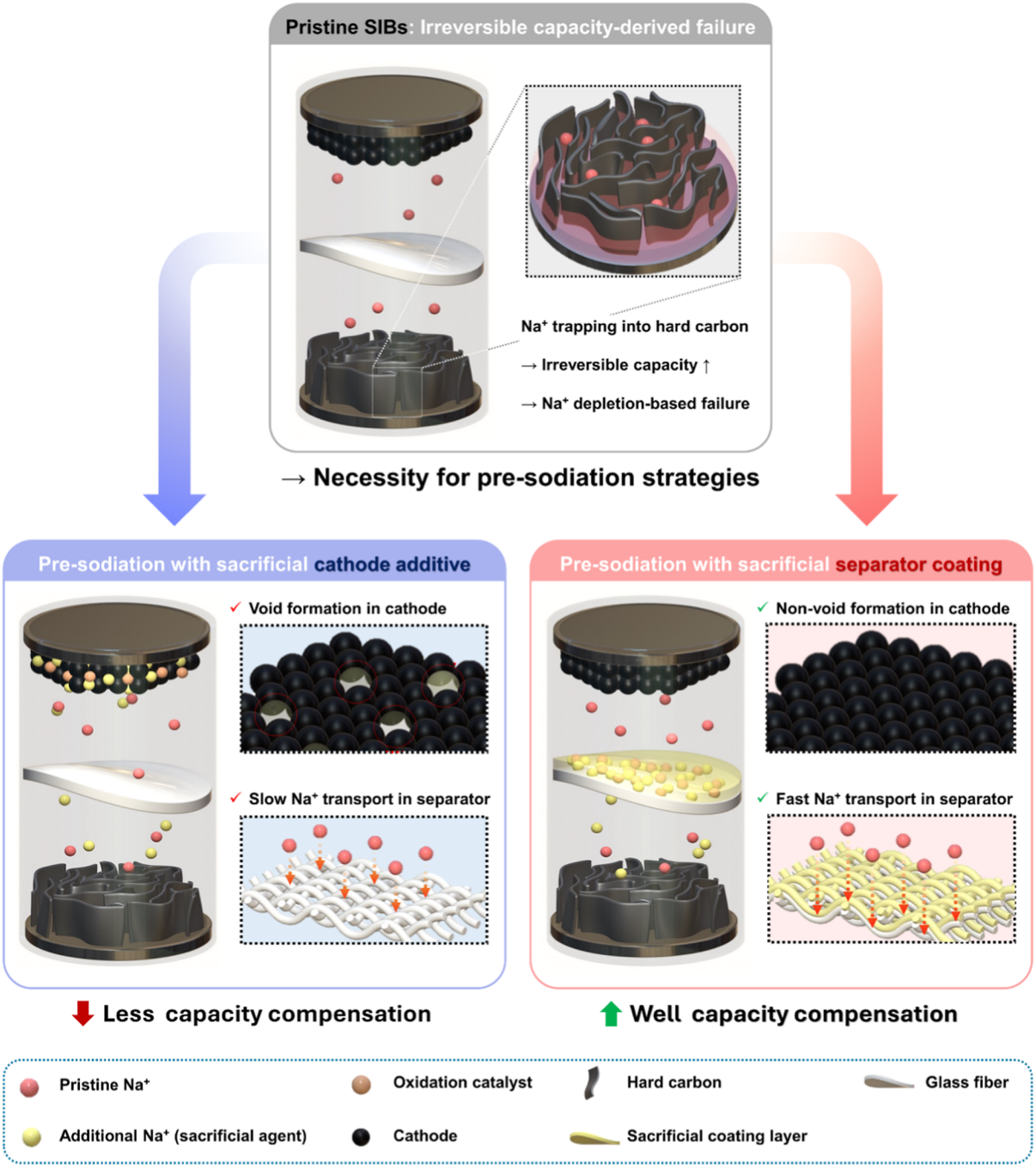

Figure 4. Illustration of Na^+ trapping in pristine SIBs, and comparison of presodiation applied as a cathode additive versus as a separator coating.

upon mixing (Figure S6). The coated morphology was examined by FE-SEM, which revealed a uniform MNC layer on the separator surface without slurry penetration (Figures S7 and S8). EDS elemental mapping further confirmed the even distribution of MnO and NaF within the coating (Figure S9), while no particles were detected on the opposite side, indicating that the coating was confined to one surface.

These results demonstrate that the MNCS is not only electrochemically effective and structurally functional but also fully compatible with conventional fabrication methods, offering a practical strategy for providing additional sodium and improving ion transport in SIB systems.

Electrochemical Performance of MNC-Coated Separator (MNCS)-Incorporated Full-Cell

To assess the effectiveness of MNCS as a functional presodiation separator in sodium-ion batteries, full-cell tests were conducted using hard carbon (HC) as the anode. Due to the intrinsic nature of HC, which stores sodium via adsorption in micropores and intercalation in disordered layers, its initial Coulombic efficiency (ICE) remains limited to approximately 75.4% (Figure S10), leading to substantial initial capacity loss in full-cell systems. To address this issue, we compared the electrochemical performance of three full-cell configurations: O3-NLNFM//PS//HC, O3-NLNFM + MNC//PS//HC, and O3-NLNFM//MNCS//HC. All three full-cell configurations

https://doi.org/10.1021/acsnano.5c16400
ACS Nano 2026, 20, 4799−4807

were assembled with an N/P ratio of 1.2. Detailed fabrication process of the full-cells is arranged in the Experimental Section.

As shown in Figure 3a, the O3-NLNFM//PS//HC full-cell exhibited an initial charge capacity of approximately 186.0 mAh g^{-1} and a discharge capacity of 104.0 mAh g^{-1} at the current rate of 0.1C (1C = 170.0 mA $g_{cathode}^{-1}$), reflecting the sodium loss due to ICL. In contrast, the O3-NLNFM + MNC//PS//HC and the O3-NLNFM//MNCS//HC full-cells showed higher charge capacities of 240.3 and 301.4 mAh $g_{cathode}^{-1}$, respectively, owing to the additional sodium provided by NaF decomposition in the MNC. The corresponding discharge capacities were 137.9 and 169.5 mAh $g_{cathode}^{-1}$, respectively, showing that the amount of sodium released from the MNC played a critical role in compensating for the initial loss. These results confirm that MNCS delivers a more effective sodium supply than direct mixing of MNC into the cathode, likely due to improved decomposition efficiency.

It is worth noting that in the half-cell configuration, where sodium metal serves as an excess sodium reservoir, the effect of MNC on the discharge capacity was difficult to distinguish. However, in the full-cell setup, the additional sodium provided by MNCS led to a clear and significant increase in discharge capacity, highlighting the practical importance of effective presodiation strategies under realistic operating conditions.

The difference in configuration also affected the interfacial resistance, as shown by the EIS results in Figure 3b. Before cycling, the charge transfer resistance (R_{ct}) of the O3-NLNFM + MNC//PS//HC full-cell was 13.25 Ω, much higher than that of the NLNFM//PS//HC full-cell (8.24 Ω), indicating that the inclusion of MNC in the cathode increases electronic resistance. Meanwhile, the O3-NLNFM//MNCS//HC full-cell exhibited the lowest R_{ct} at 4.26 Ω. This configuration also showed the lowest electrolyte resistance (R_e) among the three, as confirmed in Figure S11. After the first cycle, although resistance increased in all cases, the trend remained the same, supporting the idea that the spatial separation of MNC via the separator prevents adverse reactions at the cathode interface. Additionally, the conductive carbon matrix within the MNCS coating helped form additional electron pathways, further facilitating charge transport.

Long-term cycling data in Figure 3c show that the O3-NLNFM//MNCS//HC full-cell maintained the highest discharge capacity over 200 cycles at 0.5C, with a capacity retention of approximately 69.5%. In comparison, the O3-NLNFM + MNC//PS//HC and O3-NLNFM//PS//HC full-cells showed lower retention values of 56.9% and 62.9%, respectively. To further evaluate practical applicability, pouch-type full-cells were fabricated using the O3-NLNFM//MNCS//HC and O3-NLNFM//PS//HC configurations. The MNCS-based pouch cell exhibited superior cycling stability over extended operation compared to the pouch cell with a PS, validating the effectiveness of MNCS in realistic SIB full-cell systems. Importantly, the undesirable phenomena of gas evolution or pouch cell swelling were almost negligible with MNCS, confirming that the decomposition of NaF in the MNCS proceeds with marginal gaseous byproducts (Figure 3d). This demonstrates that MNCS enables both high-performance operation and reliable SIB full-cell integration without additional complexity in process or design.

The rate capability of each full-cell was evaluated after the initial formation cycle (Figure 3e). It was verified that the O3-NLNFM//MNCS//HC full-cell delivered outstanding fast charge/discharge performance compared to that of both the O3-NLNFM//PS//HC and the O3-NLNFM + MNC//PS//HC full-cells. Even at a high current rate of 8C, the capacity of the O3-NLNFM//MNCS//HC full-cell was retained to 78.1 mAh $g_{cathode}^{-1}$, while O3-NLNFM//PS//HC and O3-NLNFM + MNC//PS//HC full-cells just delivered 34.2 and 11.3 mAh $g_{cathode}^{-1}$, respectively.

Notably, the O3-NLNFM + MNC//PS//HC full-cell exhibited a lower capacity than the O3-NLNFM//PS//HC full-cell, indicating the drawback of directly mixing the sacrificial material with cathode particles. This suggests that physical contact between the MNC and the cathode layer may disrupt the electrode network, hinder charge transport, and lead to resistive accumulation during high-rate operation. In contrast, the MNCS structure avoids such issues by isolating the MNC on the separator, enabling facile sodium supply with a negligible impact on the cathode material.

A summarized schematic of the presodiation strategy is shown in Figure 4. The low initial Coulombic efficiency of the HC anode results in irreversible sodium loss during the first cycle, limiting the available capacity and reducing the overall energy density in full-cell configurations. To compensate for this sodium deficiency, we applied the MNC that releases additional sodium through the catalytic decomposition of NaF during the initial charge.

Two integration methods were examined: incorporating the MNC directly into the cathode and coating it onto the separator. In the case of direct mixing of MNC into the cathode, it leads to void formation in the cathode after NaF decomposition and reduced catalytic activity due to the limited MnO−NaF contact. In contrast, the MNCS where the MNC is coated onto the cathode-facing side of the separator maintains interfacial reactivity while avoiding adverse effects on the cathode. This configuration not only ensures efficient sodium delivery but also improves ion mobility across the separator, contributing to the enhanced rate capability and stable cycling.

CONCLUSION

In this work, we developed a low-cost and effective functional presodiation separator, enabling both enhanced energy density and stable cycling performance of the SIB full-cell. The MnO@NaF composite (MNC), prepared with Super P via high-energy ball milling, served as a sacrificial sodium source by promoting the catalytic decomposition of NaF during the initial charge. When coated onto the separator facing the cathode, the MNC enabled spatial decoupling from the active electrode, thereby preventing interfacial side reactions while ensuring efficient sodium delivery and improved ion transport. Notably, the MNC-coated separator (MNCS) is composed of air-stable and low-cost MnO and NaF precursors and can be fabricated by using standard slurry-coating methods, offering excellent compatibility with existing cell manufacturing processes.

With this configuration, the full-cell of the O3-NLNFM//MNCS//HC delivered an initial discharge capacity of 169.5 mAh g^{-1}, more than double that of the control cell with a pristine separator (104.0 mAh g^{-1}), effectively compensating for the sodium loss associated with the low initial Coulombic efficiency of the hard carbon anode. The O3-NLNFM//MNCS//HC full-cell also exhibited excellent rate capability and maintained a capacity retention of approximately 69.5% after 200 cycles at 0.5C, compared to 62.9% for the O3-NLNFM//PS//HC full-cell and 56.9% for the O3-NLNFM +

https://doi.org/10.1021/acsnano.5c16400
ACS Nano 2026, 20, 4799−4807

MNC//PS//HC full-cell. Furthermore, pouch-type full-cell tests confirmed the gas-free nature of the NaF decomposition and showed that MNCS enables stable long-term cycling as well as compatibility with practical processing conditions.

These results clearly demonstrate that MNCS offers a structurally optimized and electrochemically effective preso-diation strategy for next-generation sodium-ion batteries. The approach not only compensates for sodium loss in full cells but also provides practical advantages in terms of material cost, fabrication accessibility, and system-level integration, offering a new design perspective for realizing high-performance SIB systems.

METHODS

Preparation of the MNC

The MNC was synthesized using MnO (Sigma-Aldrich, 99%) and NaF (Alfa Aesar, 99%) as a precursor in a molar ratio of 1:2, with 20 wt % Super P (TIMCAL), for a total weight of 5g. The precursors were sealed in the Ar-filled glovebox to prevent water contamination and then mixed using a high-energy ball milling with silicon nitride balls at 500 rpm for 12 h, which reduced the particle size and increased the contact between MnO and NaF.[11]

Preparation of the Electrode

To prepare the cathode electrode, the NLNFM slurry was made by mixing active material ($Na[Li_{0.05}(Ni_{0.25}Fe_{0.25}Mn_{0.5})_{0.95}]O_2$), Super P, and poly(vinylidene fluoride) (PVDF, Kureha, KF-1100) in a weight ratio of 85:7.5:7.5 using NMP (Junsei Chemical) as the solvent. For the NLNFM + MNC slurry, MNC, PVDF, and Super P were added to the NLNFM slurry in a weight ratio of 8:1:1, with the mass ratio of MNC to NLNFM set at 1:3. Then, the NLNFM and NLNFM + MNC slurry was cast onto an aluminum current collector using blade coating and dried at 100 °C for 12 h in the vacuum oven. The HC electrode was prepared by making slurry with HC active material, PVDF, and Super P in a weight ratio of 8:1:1 using NMP as the solvent. This slurry was cast onto a copper current collector using blade coating and dried at 80 °C for 12 h in the vacuum oven. Finally, to prepare the MNCS, a slurry was made with MNC, PVDF, and Super P in a weight ratio of 8:1:1 using NMP as the solvent. The slurry was cast onto glass fiber (Whatman GF/F) using blade coating and dried at 60 °C for 12 h in the vacuum oven.

Material Characterization

The morphologies and particle sizes of MNC were analyzed using scanning transmission electron microscopy (STEM, JEOL company, ARM-200F) and field emission scanning electron microscopy (SEM, JEOL company, JSM 7000F). The MNC and NLNFM were analyzed by using X-ray diffraction (XRD, PANalytical, Empyrean) with Mo Kα radiation (λ = 0.7093 Å). The measurements were conducted with a step size of 0.016° over a 2θ range of 4.5−35.0°, and the patterns were converted to angles corresponding to Cu Kα radiation (λ = 1.5417 Å). X-ray photoelectron spectroscopy (XPS, Thermo Fisher Scientific, ESCALAB-250) was employed to the characterize of MNC. The valence states of Mn in the structure of MNC were determined from XANES analysis performed on beamline 7D at the Pohang Accelerator Laboratory (PAL), South Korea. The Mn K-edge spectra were collected in transmission mode with an electron energy of 2.5 GeV and a current of 200 mA. Mn reference spectra were simultaneously obtained from Mn metal foil. Raman spectroscopy was performed on the PS and MNCS after a 24 h immersion in the electrolyte, using a 532 nm laser at 7 mW (Thermo Fisher, DXR3xi). The spectra were recorded over a wavelength range of 50−1800 cm^{-1} with a resolution of 1 cm^{-1}. The volume and surface resistivity of the NLNFM and NLNFM + MNC were measured using an electrode measurement system (Hioki, RM9004). The Na^+ ion transference number (t_{Na^+}) of PS and MNCS was measured using chronoamperometry (CA) and electrochemical impedance spectroscopy (EIS). Then, the t_{Na^+} was calculated using the following equation, eq 2.[20] In this equation, I_{ss} and I_0 are steady-state and initial current, respectively, R_{ss} and R_0 are the steady-state and initial interfacial resistance at the Na/Na symmetric cell, respectively, and ΔV is the constant applied voltage (10 mV).

$$t_{Na^+} = \frac{I_{ss}(\Delta V - I_0 R_0)}{I_0(\Delta V - I_{ss} R_{ss})} \quad (2)$$

Electrochemical Measurements

CR2032 (Welcos) cells were fabricated using the cathode electrode (NLNFM or NLNFM + MNC), anode electrode (Na metal or hard-carbon), a separator (PS or MNCS), and an electrolyte (1 M of $NaPF_6$ in ethylene carbonate (EC): propylene carbonate (PC) in a volume ratio of 1:1 with 5% fluoroethylene carbonate (FEC)). All cells were assembled in an argon-filled glovebox (O_2 and H_2O <1.0 ppm). In the half-cell system, the cathode had a diameter of 12 mm, the Na metal anode had a diameter of 14 mm, and the separator had a diameter of 18 mm. The galvanostatic charge tests of NLNFM//PS//Na, NLNFM + MNC//PS//Na, and NLNFM//MNCS//Na were performed at 0.1C in the voltage range of 1.95−4.8 V for the first cycle and 0.5C for the following cycles in the voltage of 1.95−4.5 V after the initial cycle. And then, for the full-cell system, the cathode also had a diameter of 12 mm, with a hard-carbon (HC) anode of 14 mm diameter and a separator of 18 mm diameter, resulting in an N/P ratio of 1.2. The galvanostatic tests of NLNFM//PS//HC, NLNFM + MNC//PS//HC, and NLNFM//MNCS//HC were also performed at 0.1C in the voltage range of 1.75−4.3 V and 1.75−4.8 V during the initial cycle and at various c-rates (0.5C, 1C, 2C, 4C, and 8C) 1.75−4.3 V, using an automatic battery charge/discharge test system (WBCS 3000, WonATech). The NLNFM//PS//HC and NLNFM//MNCS//HC pouch cells, used to manufacture mono-layered pouch cells, were assembled with NLNFM (3.0 × 4.0 cm) and HC (3.2 × 4.2 cm) electrodes, utilizing 1 M $NaPF_6$ in EC:PC (1:1 v/v) with 5 wt % FEC as the electrolyte. The electrodes, along with a separator (3.5 × 4.5 cm), were vacuum-sealed in an aluminum pouch in a dry room with a dew point below −70 °C. After a 24 h rest period, cell formation was initiated at 0.1C in the voltage range of 1.75−4.8 V for the first cycle, followed by cycling at 0.5C in the voltage range of 1.75−4.3 V using a WBCS3000L system (WonATech).

ASSOCIATED CONTENT

Supporting Information

The Supporting Information is available free of charge at https://pubs.acs.org/doi/10.1021/acsnano.5c16400.

Characterizations (digital images, SEM images, TEM image, XRD patterns, XPS spectra, Raman spectra, XANES spectra), electrochemical behaviors, and electrochemical performances (PDF)

AUTHOR INFORMATION

Corresponding Authors

Young-Jun Kim − *SKKU Institute of Energy Science and Technology (SIEST), Department of Nano Science and Technology, SKKU Advanced Institute of Nano Technology (SAINT), and Advanced Center for Convergence Energy Storage System, Sungkyunkwan University, Suwon 16419, Republic of Korea;* orcid.org/0000-0002-9801-3066; Email: yjkim68@skku.edu

Jongsoon Kim − *Department of Energy Science, Sungkyunkwan University, Suwon 16419, Republic of Korea; SKKU Institute of Energy Science and Technology (SIEST), Sungkyunkwan University, Suwon 16419, Republic of Korea;* Email: jongsoonkim@skku.edu

https://doi.org/10.1021/acsnano.5c16400
ACS Nano 2026, 20, 4799−4807

Ki Jae Kim − *Department of Energy Science, Sungkyunkwan University, Suwon 16419, Republic of Korea; SKKU Institute of Energy Science and Technology (SIEST), Sungkyunkwan University, Suwon 16419, Republic of Korea;* orcid.org/0000-0002-2166-7467; Email: kijaekim@skku.edu

Authors

Sang Jae Park − *Department of Energy Science, Sungkyunkwan University, Suwon 16419, Republic of Korea*

Sang-Yeop Lee − *Department of Energy Science, Sungkyunkwan University, Suwon 16419, Republic of Korea; SKKU Institute of Energy Science and Technology (SIEST), Sungkyunkwan University, Suwon 16419, Republic of Korea*

Yong Min Kim − *Department of Energy Science, Sungkyunkwan University, Suwon 16419, Republic of Korea*

Jungmin Kang − *Department of Energy Science, Sungkyunkwan University, Suwon 16419, Republic of Korea; SKKU Institute of Energy Science and Technology (SIEST), Sungkyunkwan University, Suwon 16419, Republic of Korea*

Jae Kwon Seo − *Department of Nano Science and Technology and SKKU Advanced Institute of Nano Technology (SAINT), Sungkyunkwan University, Suwon 16419, Republic of Korea*

Complete contact information is available at: https://pubs.acs.org/10.1021/acsnano.5c16400

Author Contributions

#S. J. P., S. -Y. L., and Y. M. K. contributed equally to this work. S. J. Park: Conceptualization, Writing—original draft, Formal analysis, Data curation. S. -Y. Lee: Writing—original draft, Investigation. Y. M. Kim: Visualization, Formal analysis. J. Kang: Formal analysis, Validation. J. K. Seo: Investigation. Y. -J. Kim: Supervision. J. Kim: Conceptualization, Writing—review and editing, Supervision. K. J. Kim: Conceptualization, Writing—review and editing, Supervision.

Funding

This work was supported by the Ministry of Trade, Industry, and Energy/Korea Evaluation Institute of Industrial Technology (MOTIE/KEIT) (RS-2024-00449748), National Research Council of Science and Technology (NST) grant (No. GTL24012-000), funded by the MSIT, Korea and the Technology Innovation Program (RS-2024-00403571, Development of high-capacity layered oxide cathode material for sodium ion battery) funded by the Ministry of Trade, Industry and Energy (MOTIE, Korea).

Notes

The authors declare no competing financial interest.

REFERENCES

(1) Kang, J.; Park, H.; Kim, H.; Jo, J. H.; Ko, W.; Lee, Y.; Myung, S. T.; Kim, J. Development of a New Mixed-Polyanion Cathode with Superior Electrochemical Performances for Na-Ion Batteries. *ACS Sustain. Chem. Eng.* **2020**, *8*, 163−171.

(2) Lee, Y.; Lim, H.; Kim, S. O.; Kim, H. S.; Kim, K. J.; Lee, K. Y.; Choi, W. Thermal Stability of Sn Anode Material with Non-Aqueous Electrolytes in Sodium-Ion Batteries. *J. Mater. Chem. A* **2018**, *6*, 20383−20392.

(3) Xiao, B.; Rojo, T.; Li, X. Hard Carbon as Sodium-Ion Battery Anodes: Progress and Challenges. *ChemSusChem* **2019**, *12*, 133−144.

(4) Ge, P.; Fouletier, M. Electrochemical Intercalation of Sodium in Graphite. *Solid State Ionics* **1988**, *28*−*30*, 1172−1175.

(5) Zhao, L.; Zhang, T.; Li, W.; Li, T.; Zhang, L.; Zhang, X.; Wang, Z. Engineering of Sodium-Ion Batteries: Opportunities and Challenges. *Engineering* **2023**, *24*, 172−183.

(6) Hu, L.; Li, J.; Zhang, Y.; Zhang, H.; Liao, M.; Han, Y.; Huang, Y.; Li, Z. Enhancing the Initial Coulombic Efficiency of Sodium-Ion Batteries via Highly Active Na_2S as Presodiation Additive. *Small* **2023**, *19*, 2304793.

(7) Matsuzaki, M.; Tatara, R.; Kubota, K.; Kuroki, K.; Hosaka, T.; Umetsu, K.; Okada, N.; Komaba, S. Application of Na_2CO_3 as a Sacrificial Electrode Additive in Na-Ion Batteries to Compensate for the Sodium Deficiency in $Na_{2/3}[Fe_{1/2}Mn_{1/2}]O_2$. *Batter. Supercaps* **2024**, *7*, No. e202400009.

(8) Sathiya, M.; Thomas, J.; Batuk, D.; Pimenta, V.; Gopalan, R.; Tarascon, J. M. Dual Stabilization and Sacrificial Effect of Na_2CO_3 for Increasing Capacities of Na-Ion Cells Based on P2-Na_xMO_2 Electrodes. *Chem. Mater.* **2017**, *29*, 5948−5956.

(9) Pan, X.; Chojnacka, A.; Béguin, F. Advantageous Carbon Deposition during the Irreversible Electrochemical Oxidation of $Na_2C_4O_4$ Used as a Presodiation Source for the Anode of Sodium-Ion Systems. *Energy Storage Mater.* **2021**, *40*, 22−30.

(10) Jo, C. H.; Choi, J. U.; Yashiro, H.; Myung, S. T. Controllable Charge Capacity Using a Black Additive for High-Energy-Density Sodium-Ion Batteries. *J. Mater. Chem. A* **2019**, *7*, 3903−3909.

(11) Liao, J.; Zhang, F.; Lu, Y.; Ren, J.; Wu, W.; Xu, Z.; Wu, X. Sodium Compensation and Interface Protection Effects of Na_3PS_3O for Sodium-Ion Batteries with P2-Type Oxide Cathodes. *Chem. Eng. J.* **2022**, *437*, 135275.

(12) Zhang, B.; Dugas, R.; Rousse, G.; Rozier, P.; Abakumov, A. M.; Tarascon, J. M. Insertion Compounds and Composites Made by Ball Milling for Advanced Sodium-Ion Batteries. *Nat. Commun.* **2016**, *7*, 10308.

(13) Gao, H.; He, M.; Guo, R.; Gallant, B. M. Electrochemical Fluoridation of Manganese Oxide by Perfluorinated-Gas Conversion for Lithium-Ion Cathodes. *Batter. Supercaps* **2021**, *4*, 1771−1780.

(14) Lacivita, V.; Wang, Y.; Bo, S. H.; Ceder, G. Ab Initio Investigation of the Stability of Electrolyte/Electrode Interfaces in All-Solid-State Na Batteries. *J. Mater. Chem. A* **2019**, *7*, 8144−8155.

(15) Zhang, L.; Batuk, D.; Chen, G.; Tarascon, J. M. Electrochemically Activated MnO as a Cathode Material for Sodium-Ion Batteries. *Electrochem. Commun.* **2017**, *77*, 81−84.

(16) Kalapsazova, M. L.; Zhecheva, E. N.; Tyuliev, G. T.; Nihtianova, D. D.; Mihaylov, L.; Stoyanova, R. K. Effects of the Particle Size Distribution and of the Electrolyte Salt on the Intercalation Properties of P3-$Na_{2/3}Ni_{1/2}Mn_{1/2}O_2$. *J. Phys. Chem. C* **2017**, *121*, 5931−5940.

(17) Viswanath, P.; Yoshimura, M. Light-Induced Reversible Phase Transition in Polyvinylidene Fluoride-Based Nanocomposites. *SN Appl. Sci.* **2019**, *1*, 1519.

(18) Jung, S.; Kim, H.; Cho, M. G.; Cho, S.; Lee, B.; Kim, H.; Park, Y.; Hong, J.; Park, K.; Yoon, G.; Seong, W. M.; Cho, Y.; Oh, M. H.; Kim, H.; Gwon, H.; Hwang, I.; Hyeon, T.; et al. Lithium-free Transition Metal Monoxides for Positive Electrodes in Lithium-ion Batteries. *Nat. Energy* **2017**, *2*, 16208.

(19) Yim, T.; Ha, H. J.; Park, M. S.; Kim, K. J.; Yu, J. S.; Kim, Y. J. A Facile Method for Construction of a Functionalized Multi-Layered Separator to Enhance Cycle Performance of Lithium Manganese Oxide. *RSC Adv.* **2013**, *3*, 25657−25661.

(20) Logan, E. R.; Dahn, J. R. Electrolyte Design for Fast-Charging Li-Ion Batteries. *Trends Chem.* **2020**, *2*, 354−366.